Lowland Technology International 2021; 23 (3): 17-28
International Association of Lowland Technology (IALT): ISSN 1344-9656

Research Paper

Prediction of Ultimate Lateral Capacity of Rigid Spiral Pile under Static Loading in Cohesionless Soil

A.Jugdernamjil [1]*, N.Yasufuku [2], and A. Alowaisy [3]

ARTICLE INFORMATION

Article history:

Received: 17 June, 2021
Received in revised form: 21 August, 2021
Accepted: 03 September, 2021
Publish on: 06 December, 2021

Keywords:

Spiral pile
1g model test
Shape factor
Winkler's model
Rear passive earth pressure

ABSTRACT

1g model test is carried out to evaluate the ultimate lateral capacity of the spiral model pile in dense and medium dense cohesionless soil. The spiral model pile is scaled down using a proper similarity equation considering the equivalent second moment of area. The equivalent second moment of the area was obtained from a four-point bending test on a flat bar and compared with a spiral bar. In order to identify the lateral capacity of the spiral model pile, the conventional pipe and flat bar model piles were conducted as well. Winkler's model was adopted to predict the rigid spiral pile's ultimate lateral capacity in cohesionless soil. A simplified model is proposed by developing ultimate lateral soil pressure. The novel shape factor for spiral was obtained for the evaluation of ultimate lateral soil pressure by considering the projected area of the pile. The projected area of the spiral pile was compared with the pipe pile. The comparison study was conducted to spiral, flat, bar, and pipe pile, respectively, for inspecting accuracy. Among the comparison, the proposed model was indicated as a more accurate model than others. The spiral pile was shown a similar performance with a flat bar in both the empirical and the experimental results.

1. Introduction

In the state of the pile foundation's art, novel types of piles have been innovated, namely helical and spiral shape piles. In piles foundation engineering and anchoring technology, the spiral pile has been studied and developed in recent years. The spiral pile is characterized with several advantages including less construction work and relatively low soil disturbance. When piles are subjected to wind force, flood and earthquake, it suffers lateral force, which in extreme cases induce an over-deflection to the piles. Using pull-out and pushing load, the spiral pile can be driven easily with natural rotation. In other words, spiral pile is recyclable. For recovering over-deflected pile, a recyclable pile is recommended because of cost-efficiency.

[1] Graduate student, Geotechnical Engineering Laboratory, Department of Civil Engineering, Faculty of Engineering, Kyushu University, Fukuoka, 819-0395, Japan, j.amarbayar@civil.kyushu-u.ac.jp, jamarbayar@must.edu.mn (*Corresponding author)
[2] Professor, Geotechnical Engineering Laboratory, Department of Civil Engineering, Faculty of Engineering, Kyushu University, Fukuoka, 819-0395, Japan, yasufuku@civil.kyushu-u.ac.jp
[3] Research Assistant Professor, Geotechnical Engineering Laboratory, Department of Civil Engineering, Faculty of Engineering, Kyushu University, Fukuoka, 819-0395, Japan, a.adel@civil.kyushu-u.ac.jp, adel.owaisi.91@gmail.com
Note: Discussion on this paper is open until March 2022

Spiral pile foundations are frequently used in soft soil profiles soil disturbance needs to be minimized. Thus, namely; some of the solar panel farms, traffic sign, guiderail, roadside advertising board have been using a spiral pile for express construction. The spiral shape of the pile is associated with low bending stiffness due to the small cross-section area compared with the circular shape pile. Therefore, when subjected to a shearing force, the pile experiences relatively higher bending moment along the pile length compared to the pipe pile. Several studies have focused on the prediction model of axial bearing capacity of the spiral bolt in the rock Hirata et al., (2005), pushing and pull-out performance of spiral pile (Sato et al., 2014; Wang and Tani et al., 2018). Jugdernamjil and Tani et al., (2020) investigated the performance of a single spiral pile using a batter spiral pile. From the experimental result of Wang and Tani et al., (2018), the optimum pitch-width ratio, the length of pile pitch L_p, divided by the width of pile B (L_p/B), was found to be equal to 4.5. This ratio has been used in this study, as shown in **Fig.1**. A model spiral pile made by twisting a flat bar into a spiral shape was fabricated for this study. It must be noted that the real scale spiral pile for the field is manufactured using cast iron due to the easiness in fabrication.

Most of the theoretical and empirical studies related to the evaluation of lateral capacity consider circular or rectangular shape piles. Broms (1964), Petrasovits and Award (1972), Fleming (1992) assumed lateral soil pressure is uniform along the pile width. However, Prasad and Chari (1999), Awad-Allah and Yasufuku (2015) considered the side frictional resistance along frontal passive earth pressure, additionally. There is a lack of research focusing on the lateral behavior of spiral piles. Consequently, developing a novel prediction simplified model for spiral shape piles is essential.

This study aims at evaluating spiral pile's lateral capacity using 1g (standard gravitational test) model test. The results are used to develop a simplified model based on Winkler's model for predicting the spiral pile's lateral capacity. The model includes proposing a shape factor for the spiral pile and optimizing the coefficient of rear passive earth pressure. The shape factor for the spiral pile was developed considering the relative projected area of the spiral pile to the conventional types of piles. The rear passive earth pressure coefficient was empirically formulated based on the lateral soil pressure experimental data in medium and dense sandy soil. It must be noted that most of the existing design models related to laterally loaded short rigid piles ignore the rear passive earth pressure. Furthermore, the efficiency of the lateral capacity of spiral shape piles is validated by comparing it to the conventional type of pipe and flat bar piles.

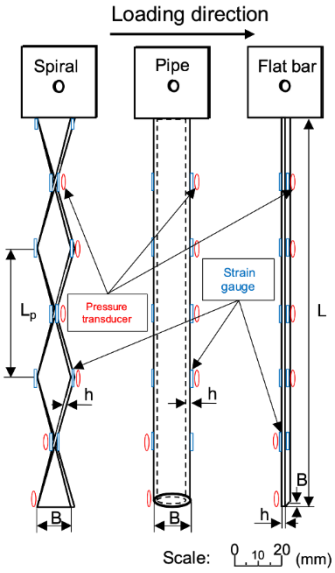

Fig.1. Schematic of model piles.

2. Experimental setup and Methodology

2.1. Experimental setup

2.1.1 Full and half-size chamber setup

A full and half-size 1g chamber model test was performed to determine the behavior of the lateral capacity. **Figure 2** shows the experimental test setup used in this study. A fabricated cuboid chamber with 420 mm depth, 600 mm length was used with a 300 mm width. The box was made using transparent acrylic plates contained in a steel frame for support. The loading device was fixed using a clamp at the center of the chamber along the loading direction for the full-size tests. In the case of half-size tests, the loading device was moved to the edge of the chamber along the loading direction. Lateral monotonic displacement was applied to the top of the pile with a loading rate of 0.01 mm/s. The applied load was measured by a load cell with 1 kN capacity.

2.1.2 Model pile

Three types of model piles were used: steel spiral, flat bar, and pipe piles for studying the lateral capacity. Both the flat bar and spiral piles have the same thickness of 3 mm, and a width of 16 mm. The outer diameter of the pipe is equal to 16 mm with 3 mm thickness. The Young's modulus of the steel model piles is 2×10^{11} N m^{-2}. The scaling of the model pile was adjusted according to the testing chamber dimensions to eliminate the boundary effect. According to Prakash (1962), the influence of the stress range extends up to 8-12 times the pile diameter in the direction of the lateral loading and 3-4 times the pile diameter in the direction perpendicular to the loading.

Considering an influence range of ten times of the pile diameter (10*B*), two types of piles varying in length were used, 144 mm and 216 mm with 16 mm width. The slenderness ratios (L/B) of the model piles were 9 and 13.5, respectively. The thickness of the piles was set to 3 mm.

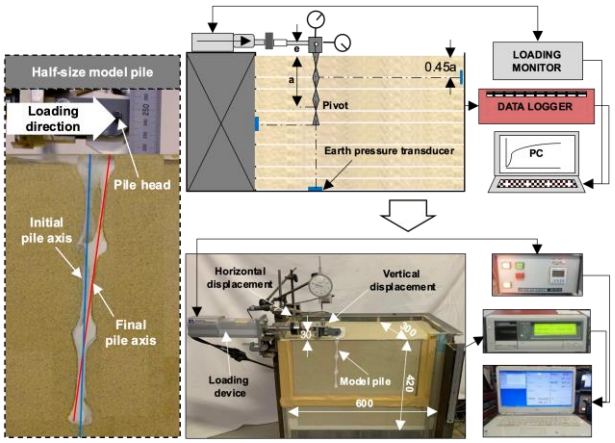

Fig.2. Experimental schematic and setup.

To determine the actual soil pressure along the pile length, pressure transducers were attached separately to the front and the rear sides of the pile, as shown in **Fig. 1**. Cables were managed by bonding on the pile surface. For the long pile, twelve strain gauges and six pressure transducers were attached, while eight strain gauges and four pressure transducers for the short pile. The location of gauges was selected on the available attachment surface of spiral shape and was illustrated in **Fig. 1**. The elevation of gauge attachment in the flat bar and pipe is followed the spiral pile. Based on preliminary tests to determine the maximum lateral soil pressure and rotation point (or pivot) of the model pile, the locations of transducers were decided. The transducers were attached facing the soil perpendicular to the loading direction. The yield load of the soil medium at 10 N for 144 mm pile and at 30 N for 216 mm pile was selected for determining the strain values. In the half-size analysis, the model piles were fabricated by cutting the full-size model piles symmetrically along the vertical axis.

Determining the representative flexural rigidity of the spiral pile is complex due to the variation of the second-moment areas along its length. The four-point bending test was conducted to evaluate the spiral's equivalent second moment of area compared with the result of the flat bar, as shown in **Fig. 3**. As shown in **Fig. 4**, the theoretical 15° tilted flat bar shows a similar result with the spiral bar using the following equations:

$$I_m = \frac{Bh \times (h^2 cos^2\theta + B^2 sin^2\theta)}{12} \quad [1]$$

where I_m is the second moment of area of the model pile, θ is the angle of a tilted flat bar with the axis, B is the width of the pile, and h is the thickness of the pile.

$$w_{max} = \frac{Pe}{24EI} \times (3L^2 - 4e^2) \quad [2]$$

where w_{max} is the central displacement, P is the load, L is the length of a span, and e is the eccentricity of a load.

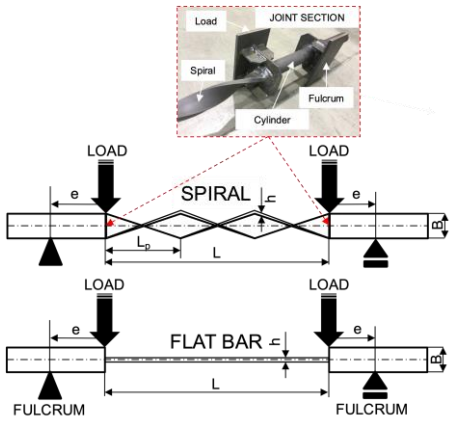

Fig. 3. Schematic of four-point bending test on spiral and flat bar.

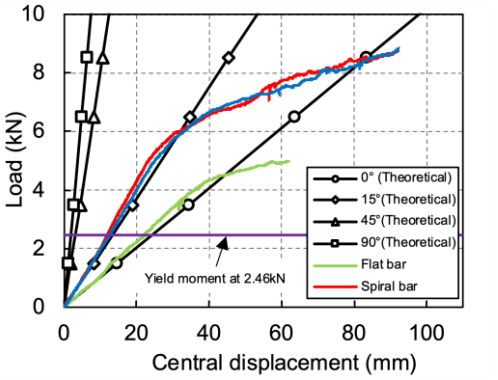

Fig. 4. Load-bending displacement relationship of experimental and theoretical analysis.

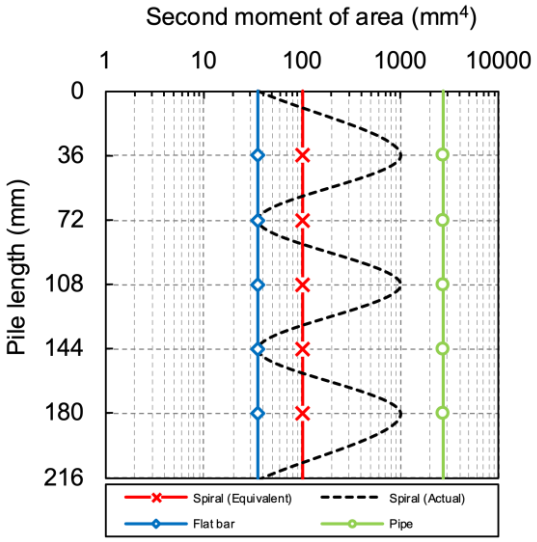

Fig. 5. Comparison of the equivalent and actual second moment of area.

The scaling of each dimension is shown in **Table 1**. The pipe and the flat bar were fabricated with the same dimensions as the spiral pile. The scaling of the prototype represented by the model pile is calculated using the equivalent second moment of the area from the four-point bending test assuming a scale factor (F), based on Wood et al., (2002):

$$\frac{E_m I_m}{E_p I_p} = \frac{1}{F^{4.5}} \quad [3]$$

where F is the scale factor, E_mI_m is the flexural rigidity of model pile, and E_pI_p is the flexural rigidity of the prototype pile. For a prototype cast iron spiral pile with a diameter of 290 mm, the scaling factor is estimated to be equal to 10 (F=10).

Table 1. Properties of spiral pile.

Parameter	Model	Prototype
Material	Steel	Cast iron
Young's modulus, E (GPa)	200	170
The second moment of area, I (m^4)	1.02×10^{-10}	3.80×10^{-6}
Flexural rigidity, EI (m^2)	20.44	64.63×10^{4}
Length, L (m)	0.144 0.216	2.6 3.9
Width, B (m)	0.016	0.29
Thickness, h (m)	0.003	0.05
Scale factor, F	1	10

Rigid and flexible piles can be classified based on the relative stiffness factor, which expresses the relation between pile flexural stiffness and soil stiffness considering the constant of horizontal subgrade reaction. If the constant of horizontal subgrade reaction increasing linearly with depth, the stiffness factor can be expressed as follows:

$$T = \sqrt[5]{\frac{E_m I_m}{n_h}} \quad [4]$$

where E_mI_m is the flexural rigidity of a model pile, and n_h is the constant of a horizontal subgrade reaction.

Piles in cohesionless soil can be considered as rigid piles if $L \leq 2T$. The values of the constant of horizontal subgrade reaction for medium and dense state conditions are 6330 and 16633 kN/m^3, respectively. The corresponding 2T values are 2.53 m and 2.08 m for the spiral pile, respectively. Furthermore, the pipe and flat bar piles can be considered as short rigid piles.

2.1.3. Material

Standard silica sand (Kumamoto sand, K-7) is used. The sand has a specific gravity of 2.63, with a friction angle of 35.8° and 41.1° at γ_d=14.2 kN/m^3 and γ_d=15.2 kN/m^3, respectively based on CD triaxial tests. The soil properties and the particle size distribution curve are shown in **Table 2** and **Fig. 6**. The uniformity coefficient of K-7 sand is 1.76.

Table 2. Physical and mechanical properties of K-7 sand.

Properties	Value
Specific gravity, Gs	2.63
Maximum dry density, ρ_{max}	1.56 g/cm^3
Minimum dry density, ρ_{min}	1.19 g/cm^3
Coefficient of uniformity, U_c	1.76
Median diameter, D_{50}	0.17 mm
Relative density, Dr	70%; 90%
Internal friction angle, φ	35.8°; 41.1°

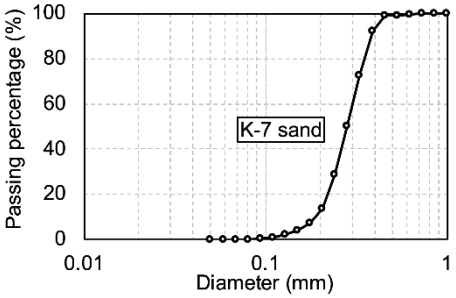

Fig. 6. Grain size distribution of K-7 sand

2.2. Methodology

2.2.1 Soil preparation

In the case of full-size analysis, earth pressure transducers for inspecting boundary effect on the front, rear, and bottom wall along the loading direction were installed before filling the sand. The height of the chamber was divided into 12 layers. For each layer the mass of soil corresponding to each relative density (70% and 90%) was determined. The free-fall steel compaction method was used to ensure uniform density through the profile. Relative density might be varied by ±3%. The sand was filled up to the bottom tip of the model pile. followed by installing the model pile in its position. The sand was filled using the same method till the top of the chamber. The lateral load was applied to the pile using a servo cylinder and measured with load cell attached to the cylinder head. The lateral load was applied with 40 mm eccentricity above the soil surface. Lateral and vertical deflection at the soil bed level was measured using LVDTs with 50 mm measurement range. Based on the result of the vertical displacement, there was no significant displacement nearly zero. The output from the load cell and the LVDT, strain gauge, earth pressure transducer was recorded using a 30-channel carrier frequency amplifier and recorded using a computer-based data acquisition system. A half-size chamber experimental test was conducted for measuring rotation points in medium and dense state sand. Similar procedure of sand filling up to pile tip was used.

However, a grease layer was applied between the half size pile and acrylic wall to reduce the friction before proceeding with filling the sand. To visualize the rotation point of the pile, the initial vertical axis line (blue-colored) on the acrylic wall and mobilized vertical axis line (red-colored) on the model pile were marked (**Fig. 1**).

2.2.2. Experimental test conditions and cases

Brom's model (1964), which is widely used for estimating the ultimate lateral capacity of the pile, was adopted. Consequently, the point where the load-deflection curve intersects with a deflection at 20% of the width of the pile (*0.2B*) is considered as the ultimate measured lateral capacity $H_{u(m)}$. Meanwhile, the soil around the pile within the range of failure wedge can be assumed to be yielded. Once the displacement reached *0.2B*, the test was terminated. Overall, 24 cases of the experimental model test were conducted in medium and dense sandy soil, including full and half-size chamber tests as shown in **Table 3**.

Table 3. Experimental test conditions.

No.	Test ID	*Dr* (%)	*L/B* ratio	Deflection (mm)
	Full-size chamber analysis			
1	Spiral 144 mm	90	9	3.2
2	Flatbar 144 mm			
3	Pipe 144 mm			
4	Spiral 216 mm		13.5	
5	Flatbar 216 mm			
6	Pipe 216 mm			
7	Spiral 144 mm	70	9	
8	Flatbar 144 mm			
9	Pipe 144 mm			
10	Spiral 216 mm		13.5	
11	Flatbar 216 mm			
12	Pipe 216 mm			
	Half-size chamber analysis			
1	Spiral 144 mm	90	9	3.2
2	Flatbar 144 mm			
3	Pipe 144 mm			
4	Spiral 216 mm		13.5	
5	Flatbar 216 mm			
6	Pipe 216 mm			
7	Spiral 144 mm	70	9	
8	Flatbar 144 mm			
9	Pipe 144 mm			
10	Spiral 216 mm		13.5	
11	Flatbar 216 mm			
12	Pipe 216 mm			

3. Performance of model piles

Figures 7 a, and b shows the typical load-deflection curves for the three different shapes of the pile with two different lengths in medium and dense sand. In a medium dense state, the lateral load capacity in the case of a spiral pile of 144 mm length is 53.8% lower than that of 216 mm spiral pile. This ratio of the lateral capacity is 33.3% and 66.7% relative to the flat bar and pipe, respectively. Meanwhile, in the dense state, the case of spiral 144 mm is 33.3% lower than the lateral load capacity obtained in the case of spiral 216 mm. This ratio is 24.5% and 56.1% for the cases of flat bar and pipe, respectively.

It is obvious that the pile slenderness ratio and bending stiffness significantly affects the lateral load capacity. The ultimate lateral load capacity of a short rigid pile is essentially provided by the mobilization of the front and the rear passive earth pressure along the pile length. In other words, it strongly depends on the cross-section of the pile. Therefore, the result of the pipe shows higher capacity than the case of the spiral and the flat bar because of higher flexural rigidity.

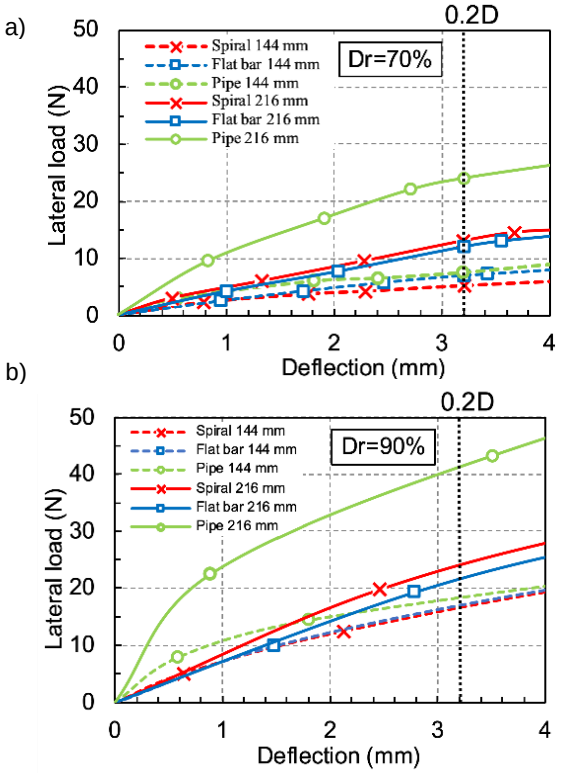

Fig. 7. Load-deflection curve a) Medium density sandy soil at *Dr*=70% b) Dense state sandy soil at *Dr*=90%.

4. Estimation of the ultimate lateral capacity

4.1. Derivation of the ultimate lateral capacity

Winkler's model is commonly used to analyze the ultimate lateral capacity of the pile that considers the modulus of subgrade reaction. The model is a 4th order differential equation (**Equation 5**). By solving the 4th order differential equation, the deflection (**Equation 6**) can be obtained as follows by integrating the ordinary differential equation:

$$EI\frac{d^4y}{dz^4} + p_u z = 0 \quad [5]$$

$$\frac{d^3y}{dz^3} = -\int \frac{p_u z}{EI} dz = -\frac{p_u z^2}{2EI} + C_1$$

$$\frac{d^2y}{dz^2} = -\int \frac{p_u z^2}{2EI} dz + C_1 = -\frac{p_u z^3}{6EI} + C_1 z + C_2$$

$$\frac{dy}{dz} = -\int \left(\frac{p_u z^3}{6EI} + C_1 z + C_2\right) dz$$

$$y = -\int \left(\frac{p_u z^4}{24EI} + \frac{C_1 z^2}{2} + C_2 z + C_3\right) dz$$

$$y = -\frac{p_u z^5}{120EI} + \frac{C_1 z^3}{6} + \frac{C_2 z^2}{2} + C_3 z + C_4 \quad [6]$$

where *EI* is the flexural rigidity, *y* is the deflection, *z* is the depth, and $C_{1\sim4}$ are the unknown constants.

Assuming the boundary conditions based on experimental modeling as shown in **Fig. 8**, the ultimate lateral capacity of pile $H_{u(p)}$ (**Equation 7**) can be obtained from the 3rd boundary condition as follows:

1st boundary condition

z=0 $V = -EI\frac{d^3y}{dz^3} = -H_u$ $\frac{d^3y}{dz^3} = C_1$ $C_1 = \frac{H_u}{EI}$

2nd boundary condition

z=0 $M = -EI\frac{d^2y}{dz^2} = -H_u \cdot e$ $\frac{d^2y}{dz^2} = C_2$ $C_2 = \frac{H_u \cdot e}{EI}$

3rd boundary condition

z=a $M = -EI\frac{d^2y}{dz^2} = 0$

$$H_{u(p)} = \frac{p_u a^3}{6(a+e)} \quad [7]$$

where *V* is the shear, *M* is the moment, p_u is the ultimate lateral soil pressure, *a* is the rotation point (or pivot), and *e* is the eccentricity of lateral load.

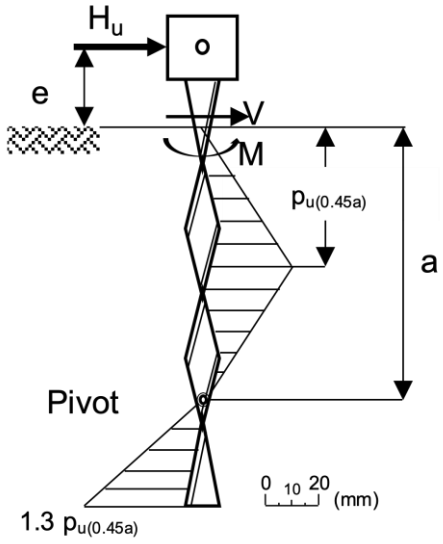

Fig. 8. Distribution of frontal and rear soil resistance of spiral pile.

4.2. Evaluation of ultimate lateral soil pressure

The ultimate lateral soil pressure can be analyzed by two components, the frontal soil resistance and side frictional resistance between soil and pile surface. Prasad and Chari (1999) proposed for predicting ultimate soil resistance for laterally loaded pile in cohesionless soil considering that two components as follows:

$$p_u = (\eta p_{max} + \xi \tau_{max})B \quad [8]$$

where η is frontal shape factors, ξ is side shape factor, p_{max} is frontal soil resistance, τ_{max} is side frictional resistance, and *B* is pile width.

In the following subsections, the shape factors and selection of models for frontal soil pressure evaluation, and coefficient of rear passive earth pressure and rotation point, were discussed.

4.2.1. Determination of the shape factor of spiral pile

The frontal pressure and side shear of the spiral pile are variable along the pile length, as shown in **Fig.10. a)**. The interaction between soil and surface of spiral and pipe is curved along the loading direction. Therefore, the spiral pile behavior is closer to that of a pipe pile compared to a square pile. Each of the frontal and side shape factors of the spiral pile was calculated as follows:

$$\eta_{Spiral} = \frac{A_{Spiral(front)}}{A_{Pipe(front)}} \times \eta_{Pipe} \quad [9]$$

$$\xi_{Spiral} = \frac{A_{Spiral(side)}}{A_{Pipe(side)}} \times \xi_{Pipe} \quad [10]$$

where $A_{Spiral(front)}$, and $A_{Pipe(front)}$ are the frontal projected area of a spiral and a pipe pile, $A_{Spiral(side)}$, and $A_{Pipe(side)}$ are the side projected area of a spiral and a pipe pile, η_{Pipe} is a pipe frontal shape factor, ξ_{Pipe} is the side shape factor of pipe pile.

The frontal projected area of the spiral pile was calculated using the sinusoidal function considering loading direction on pile. Meanwhile, the side projected area can be obtained from cosinusoidal function as expressed in **Equation 11 and 12** considering the spiral's dimensions as illustrated in **Fig. 9**.

$$A_{Spiral(front)} = \sum_{i=1}^{n} \left(L_p \times h + 2 \times \int_0^{L_p} w \sin\frac{\pi}{L_p} dy\right)_i = \frac{nL_p(\pi h + 4w)}{\pi} \quad [11]$$

$$A_{Spiral(side)} = \sum_{i=1}^{n} \left(L_p \times h + 2 \times \left(\int_0^{\frac{L_p}{2}} w\cos\frac{\pi}{L_p}dy + \int_{\frac{L_p}{2}}^{L_p} -w\cos\frac{\pi}{L_p}dy \right) \right)_i = \frac{nL_p(\pi h + 4w)}{\pi} \quad [12]$$

where n is the number of a pitch, w is the length of the spiral wing, L_p is the length of a pitch, and h is the thickness. of a spiral pile.

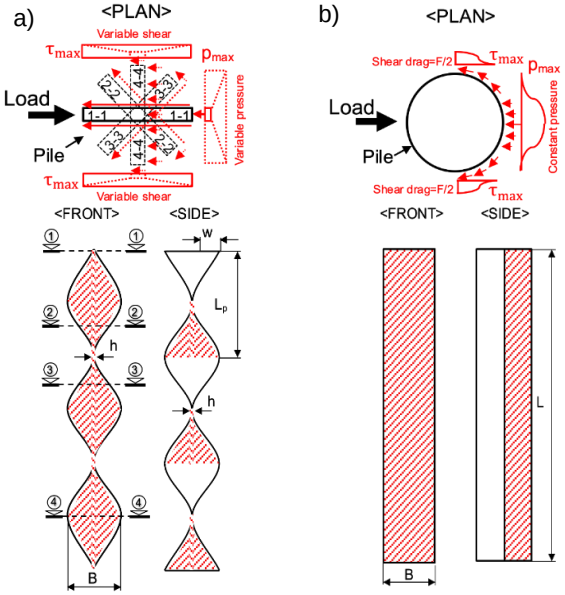

Fig. 9. The projected area of a) spiral and b) pipe pile.

By substituting **Equation 11 and 12** to **Equation 9** and **10**, the frontal and side shape factors can be expressed as follows:

$$\eta_{Spiral} = \frac{A_{Spiral(front)}}{A_{Pipe(front)}} \times \eta_{Pipe} = \frac{nL_p(\pi h + 4w)}{LB\pi} \times \eta_{Pipe} \quad [13]$$

$$\xi_{Spiral} = \frac{A_{Spiral(side)}}{A_{Pipe(side)}} \times \xi_{Pipe} = \frac{nL_p(\pi h + 4w)}{LB\pi} \times \xi_{Pipe} \quad [14]$$

where L is the length of a pipe pile, and B is the width of a pipe pile.

The novel frontal and side shape factor for spiral pile was developed using a projected area that compared with the existing shape factors of pipe cross-sectional pile as demonstrated in **Table 4**.

4.2.2. Frontal and side soil resistance

To identify the difference of actual lateral soil pressure across the pile width corresponding to the three different shapes of piles, earth pressure transducers were used to measure the lateral soil pressure. Based on the results, the variation of the lateral soil pressure can be delineated, as shown in **Fig. 10**. To determine the passive earth pressure of pile at the front and rear sides, several models including Broms (1964) and Fleming et al., (1992) were adopted. Among by normalizing p_{max} by $3\gamma K_p$ and $\gamma K_p{}^2$, the $p_{max}/3\gamma K_p$ was indicated that the value nearly inclined line as demonstrated in **Figs 11 a, and b**. Thus, frontal, and rear soil resistance can be analyzed by $3\gamma K_p$.

Table 4. Shape factor.

Pile shape	Projected area, A (mm^2)		Shape factor, η, and ξ	
	Frontal	Side	Frontal	Side
Spiral	2436	2436	0.6*	0.7*
Flat bar	3456	648	1.0**	0.4*
Pipe	3456	3456	0.8**	1.0**
Square	3456	3456	1.0**	2.0**

*) Present study
**) Briaud and Smith, (1983)

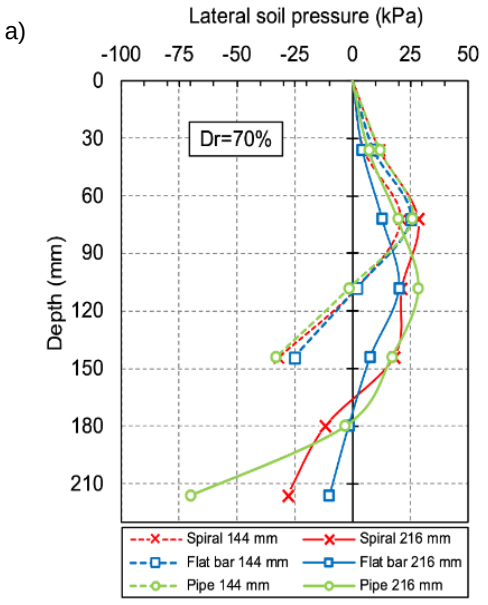

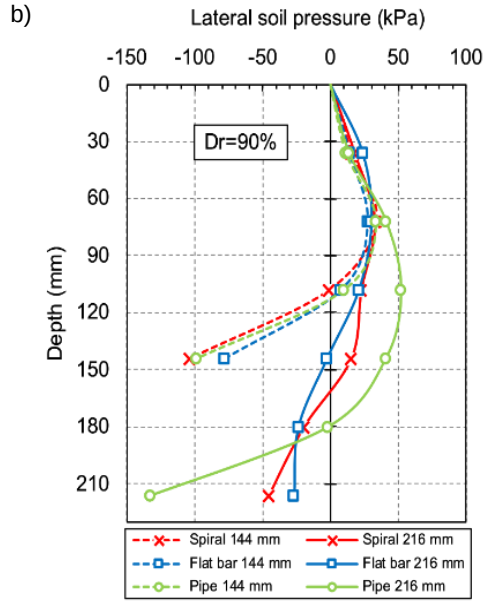

Fig. 10. Variation of the lateral soil pressure with depth a) Medium density state sandy soil *Dr*=70% b) Dense state sandy soil *Dr*=90%.

a)

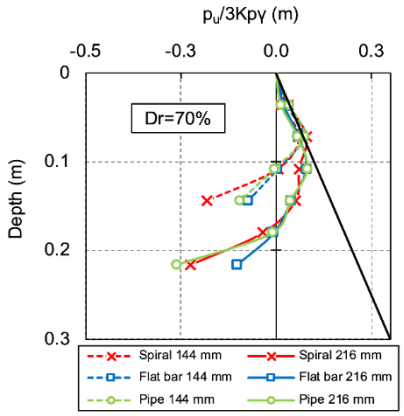

b)

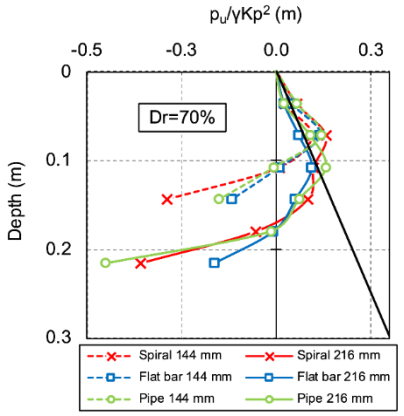

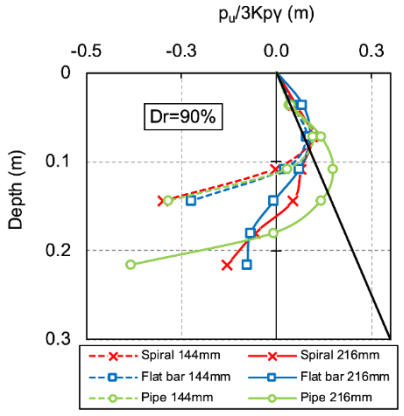

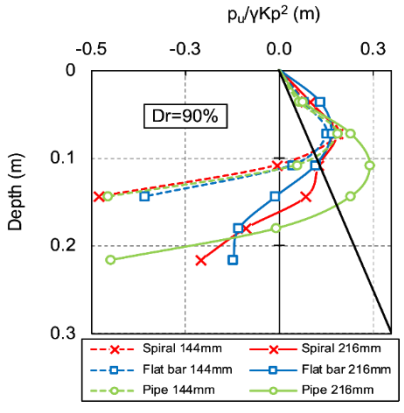

Fig. 11. Distribution $p_u/3K_p\gamma$ and $p_u/\gamma K_p^2$ with depth a) *Dr*=70% b) *Dr*=90%.

It must be noted that most of the preceding studies on the evaluation of the lateral soil pressure, ignored the rear passive earth pressure. Based on the result of measuring actual lateral soil pressure from the 1g model test, the rear passive earth pressure of the pile was found to be one of the major factors affecting the lateral capacity. In order to consider the rear passive earth pressure, the coefficients are obtained by using magnitude in frontal and rear actual passive earth pressure from test results (**Table 5**). The following expression was performed for obtaining coefficients as follows:

$$\zeta = \frac{p_r}{p_{f\ (0.45a)}} \quad [15]$$

where $p_{f(0.45a)}$ *is the* magnitude of a maximum frontal passive pressure at depth equal to be *0.45a*, and p_r is the magnitude of a maximum rear passive pressure.

Table 5. Coefficient of rear passive earth pressure.

Pile shape	Rear passive pressure co-efficient, ζ			
	Dr=70%		*Dr*=90%	
	L/B=9	*L/B*=13.5	*L/B*=9	*L/B*=13.5
Spiral	1.1	1.0	2.7	1.3
Flat bar	1.2	0.5	2.2	1.0
Pipe	1.5	2.4	2.9	3.4

By considering the analysis of frontal and rear passive earth pressure and coefficient of rear passive earth pressure, respectively, the frontal soil resistance can be evaluated as the following equation:

$$p_{max} = \left(3K_p + \zeta 3K_p\right)\gamma_d \quad [16]$$

where K_p is Rankine's passive earth pressure $K_p=tan^2(45+\varphi/2)$, ζ is the coefficient of rear passive earth pressure, and γ_d is a dry unit weight soil.

The lack of data on the actual measured maximum side frictional resistance, it can be found in literature as the ultimate vertical shear resistance as follows:

$$\tau_{max} = K_f \gamma_d \tan\delta \quad [17]$$

where K_f is the lateral earth pressure coefficient for friction that *0.7* times coefficient of earth pressure at rest $K_0=1-sin\varphi$, δ= interface friction angle between soil and pile.

4.2.3. Ultimate lateral soil pressure for spiral pile

By substituting **Equation 13~17** to **Equation 8**, the ultimate soil pressure for spiral pile can be obtained by considering such as pile dimension, shape factor, Rankine's passive earth pressure, as follows:

$$p_u = nL_p(\pi h + 4w)\left(\eta_{Pipe}3K_p(1+\zeta) + \xi_{Pipe}K_f \tan\delta\right)\gamma_d(\pi L)^{-1} \quad [18]$$

where n is the number of pitch, w is the length of a spiral wing, L_p is the length of a pitch, h is the thickness of a spiral pile, L is the length of a pipe pile, B is the width of a pipe pile, η_{Pipe} and ξ_{Pipe} are the frontal and side shape factor of a pipe pile, K_p is Rankine's passive earth pressure ($K_p=tan^2(45+\varphi/2)$), ζ is the coefficient of a rear passive earth pressure, γ_d is the dry unit weight soil, K_f is the lateral earth pressure coefficient for friction that *0.7* times coefficient of earth pressure at rest ($K_0=1-sin\varphi$), and δ is the interface friction angle between soil and pile surface.

4.3. Rotation point of the pile using visual analysis approach

A half-size chamber experimental test was conducted for measuring rotation points in medium and dense state sand. The rotation angle for **Equation 20** is shown in **Table 6**. The rotation point of the pile can be calculated following equation using the trigonometric function:

$$tan\,\alpha = \frac{0.2B}{a+e} \quad [19]$$

$$a = \frac{0.2B}{\alpha} - e \quad [20]$$

where *0.2B* is a horizontal displacement, α is rotation angle, and e is loading eccentricity.

Table 6. Rotation degree from half-size chamber analysis.

Pile type	*L/B*	Relative density	
		Dr=70%	*Dr*=90%
Spiral	9	1.33°	1.38°
	13.5	0.99°	1.02°
Flat bar	9	1.33°	1.38°
	13.5	0.96°	1.00°
Pipe	9	1.33°	1.38°
	13.5	0.97°	1.01°

Visual observation of pile rotation under lateral was shown in **Fig. 12**. The image of the case spiral 144 mm at *Dr*=90% was displayed by different color due to the using background flash.

a) Spiral pile

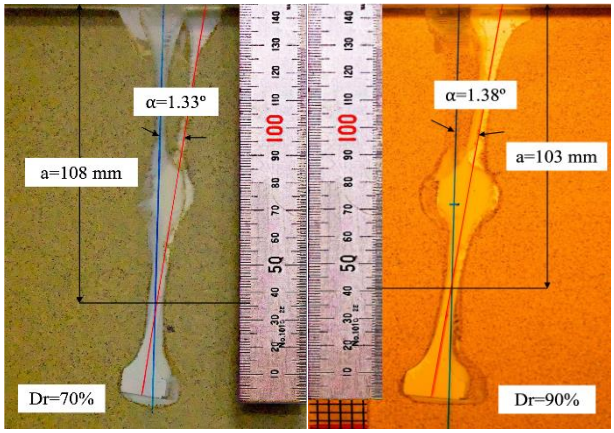

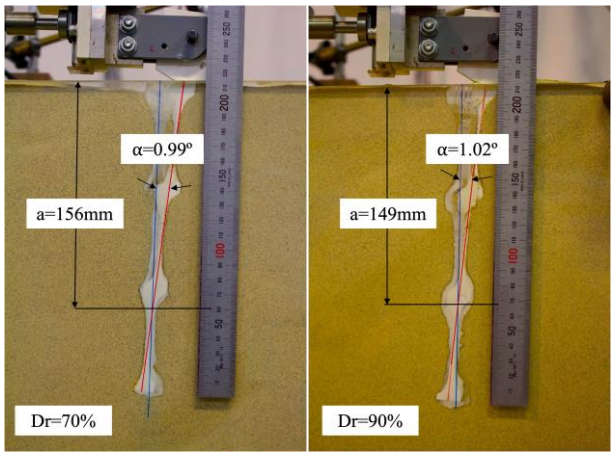

b) Flat bar

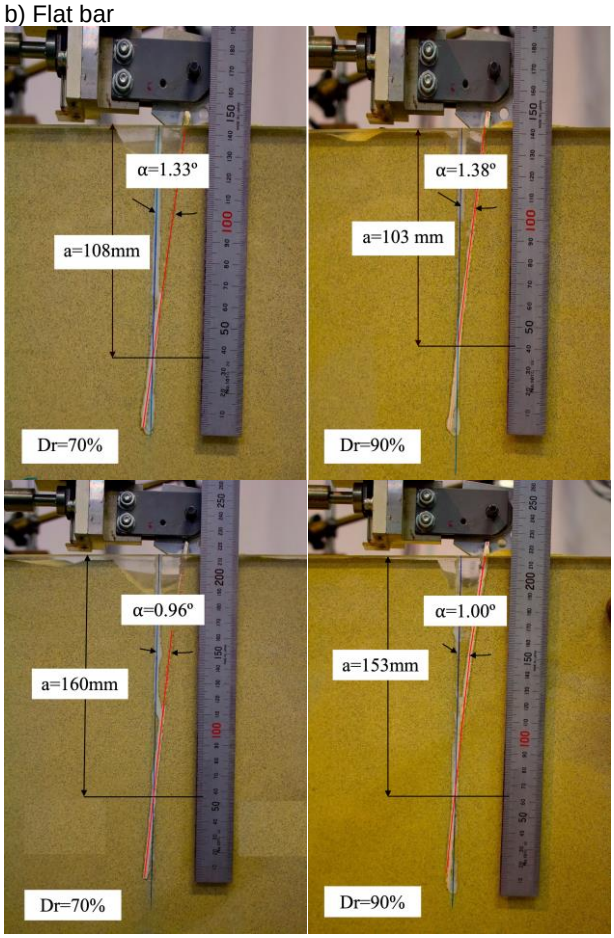

c) Pipe pile

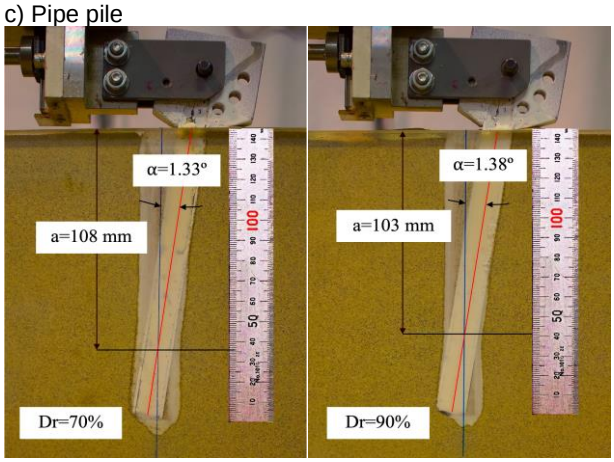

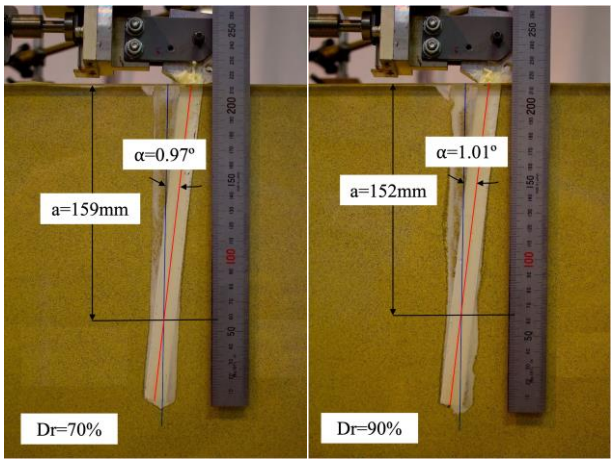

Fig. 12. Rotation point of the pile (Half-size analysis).

4.4. Proposed formula of ultimate lateral capacity of spiral pile

By substituting **Equation 18** and **20** to **Equation 7**, the ultimate lateral capacity of the spiral pile can be obtained considering as the pile dimension, shape factor, coefficient of rear passive earth pressure around the pile, Rankine's passive earth pressure, and rotation point, and internal friction angle as follows:

$$H_{u(p)} = nL_p(\pi h + 2w)\big(3K_p\eta_{Pipe}(1+\zeta) + \xi_{Pipe}K_f\,tan\,\delta\big)\gamma_d(0.2B - e\alpha)^3(1.2\pi BL\alpha)^{-2} \quad [21]$$

where n is the number of a pitch, w is the length of the spiral wing, L_p is the length of the pitch, h is the thickness of a spiral pile, $0.2B$ is a horizontal displacement, α is rotation angle, e is the loading eccentricity, L is the length of a pipe pile, B is the width of a pipe pile, η_{Pipe} and ξ_{Pipe} are the frontal and side shape factor of a pipe pile, K_p is Rankine's passive earth pressure ($K_p = tan^2(45+\varphi/2)$), γ_d is the dry unit weight soil, , K_f is the lateral earth pressure coefficient for friction that 0.7 times coefficient of earth pressure at rest ($K_0 = 1-sin\varphi$), and δ is the interface friction angle between soil and pile surface.

5. Verification of proposed model

The proposed model shows a higher accuracy, as shown in **Fig.13**. In order to evaluate the results, the error of the predictability is calculated to control the accuracy of the predicted method. The percentage of error is calculated as follows:

$$\varepsilon\,(\%) = \left(\frac{H_{u(p)} - H_{u(m)}}{H_{u(m)}}\right) \times 100 \quad [22]$$

where $H_{u(p)}$ is the predicted ultimate lateral capacity, and $H_{u(m)}$ is the measured ultimate lateral capacity of the pile.

The accuracy of the proposed model was compared with the previous models that developed under laboratory and field test reported in the literature. Five models have been adopted in this study to conduct the comparison study. Models are presented in **Table 7** with chronograph. Based on the comparison result in spiral and flat bar and pipe, the proposed model was shown higher accuracy than others (**Figs. 14, 15, and 16**).

Table 7. Predicting models of lateral pressure on the pile.

Model	Equation of p_u
Broms (1964)	$p_u = 3K_p\gamma_d B$
Petrasovits and Award (1972)	$p_u = (3.7K_p - K_a)\gamma_d B$
Verruijt *(1995)*	$p_u = (K_p - K_a)\gamma_d B$
Prasad and Chari (1999)	$p_u = [10^{(1.3\,tan\,\varphi+0.3)}]\gamma_d B$
Awad-Allah and Yasufuku (2015)	$p_u = [\eta(K_p^2 - K_a) + \xi K_f\,tan\,\delta]\gamma_d B$
Proposed model	$p_u = [\eta(3K_p + \zeta 3K_p) + \xi K_f\,tan\,\delta]\gamma_d B$

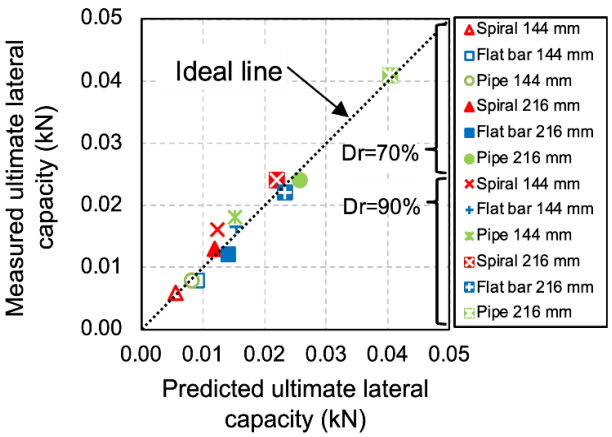

Fig. 13. Comparison of predicted and measured ultimate lateral capacity of pile.

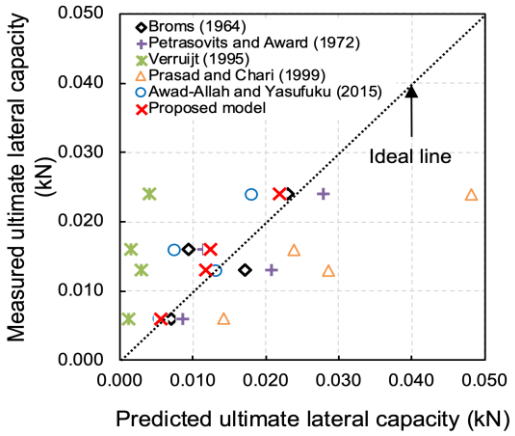

Fig. 14. Comparison between the proposed model and previous models for spiral pile.

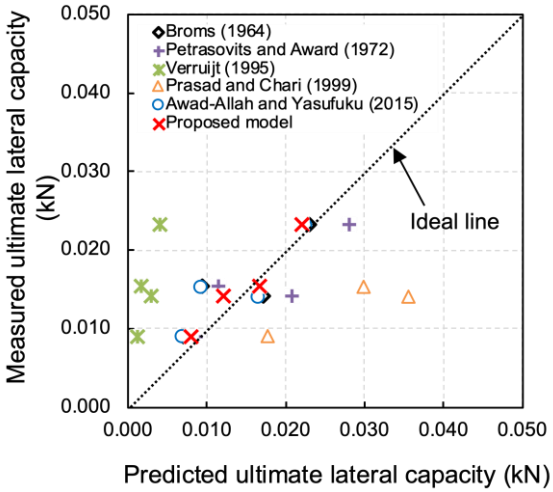

Fig.15. Comparison between the proposed model and previous models for flat bar pile.

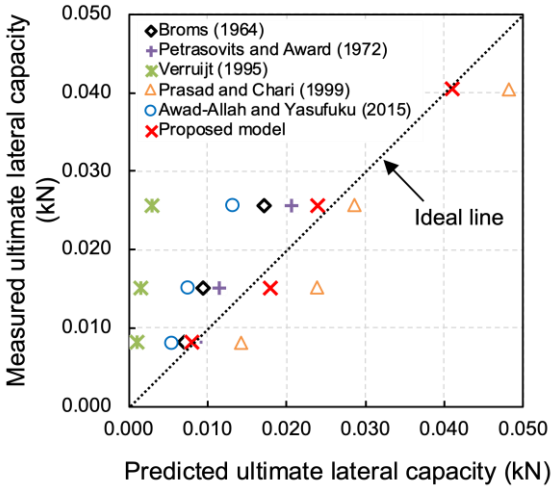

Fig.16. Comparison between the proposed model and previous models for pipe pile.

6. Conclusions

In this study, a novel shape factor and coefficient of rear passive pressure around the pile and rotation point for evaluating the ultimate lateral capacity was proposed. The experimental test was performed to confirm the reliability of the proposed model. The conclusions of this study can be summarized as follows:

1. To evaluate the ultimate lateral capacity of the rigid spiral pile, the 1g model test has been performed in dense cohesionless soil. Model piles dimension was scaled down using proper scaling law. Spiral's equivalent second moment of the area has been obtained from a four-point bending test comparing with a flat bar. Pipe and flat bar model piles are conducted to investigate the efficiency of the ultimate lateral capacity of the spiral.
2. The ultimate lateral capacity of the spiral model pile was shown as the similar lateral capacity of the flat bar pile. It is obvious that the pile slenderness ratio and bending stiffness, relative density markedly affects the lateral load capacity. The ultimate lateral load capacity of a short rigid pile is essentially provided by the mobilization of front and rear passive earth pressure along the pile length; in another way, it is significantly dependent on the cross-sections of piles.
3. One of the available models for evaluating the ultimate lateral capacity of the pile is Winkler's model. By derivation of the 4th order differential equation and assuming boundary conditions of the 1g model test program, the ultimate lateral capacity can be analyzed. Additionally, the shape factor, coefficient of rear passive earth pressure, and rotation point were taken into account. Based on the comparison result in spiral and flat bar and pipe, the proposed model was shown higher accuracy than others
4. Considering the projected area of spiral shape, the novel shape factor was proposed. In order to evaluate frontal soil pressure, the proper model was selected based on the experimental evidence. Rear passive earth pressure and side shear resistance, which are ignored in most of the evaluation of the lateral capacity of the pile foundation. Those components play a significant role in the lateral bearing capacity of the pile. To account for the rear passive pressure, the coefficients are obtained directly from an actual earth pressure measurement. Additionally, the evaluation of the rotation point of the pile was proposed using visual observation through half-size chamber analysis.

Acknowledgments

The authors express their gratitude to the Mongolia-Japan higher Engineering Education Development project (M-JEED) for fund. Also, the authors are grateful to associate professor Ryohei Ishikura, and laboratory technical assistant Mr. Michio Nakashima and members Mr. Yosuke Tani, Mr. Takahiro Kurokawa, Mr. Makoto Nagata of HINODE Co., Ltd for their support.

References

Awad-Allah, M. F., Yasufuku, N., Omine, K., 2012. Influence of Active Earth Pressure and Side Shear Resistance on Ultimate Horizontal Pile Capacity. The

9th Int. Conf. on Testing and Design Methods for Deep Foundations. Kanazawa, Japan.

Briaud, J. L. and Smith, T. D., 1983. Using the pressuremeter curve to design laterally loaded piles. Proc. 15th Offshore Tech Conf, Houston, US, **4501**: 495-502.

Broms, BB., 1964. Lateral resistance of piles in cohesive soils. J. Soil Mech. Found. Div., **90**(2): 27–64.

Fleming, W. G. K., Weltman, A. J., Randolph, M. F. and Elson, W. K., 1992. Piling engineering. Surrey University Press, London, UK.

Hirata, A., Kokaji, S., Kang, S. S. and Goto, T., 2005. Study on the Estimation of Axial Resistance of Spiral Bar Based on Interaction with Ground. Shigen-to-Sozai, **121**: 8. (in Japanese).

Jugdernamjil, A. and Yasufuku, N., Kurokawa, T., Tani, Y., Nagata, M., 2021. Experimental observation on the ultimate lateral capacity of vertical-batter screw pile under monotonic loading in cohesionless soil. Proc. 2nd International Press-in Engineering (ICPE2021), Kochi, Japan: 158-165.

Jugdernamjil, A. and Yasufuku, N., Tsamba, Ts., 2021. Ultimate Lateral Capacity of Rigid Spiral Pile under Monotonic Loading in Dense Sandy Soil. 31st Int. Ocean and Polar Engineering Conference (ISOPE2021), Rhodes, Greece: 1361-1368.

Kulhawy, F. H., 1984. Limiting tip and side resistance: Fact or fallacy. Proc. Symp. on Design and Analysis of Pile Found, ASCE, New York, 80–98.

Kulhawy, F. H., 1991. Drilled shaft foundations. Foundation engineering handbook. 2, Van Nostrand Reinhold, New York.

Kulhawy, F. H., Trautmann, C. H., Beech, J. F., O'Rourke, T. D., McGuire, W., Wood, W. A. and Capano, C., 1983. Transmission line structure foundations for uplift-compression loading. Rep. No, EL-2870, Electric Power Research Institute, Palo Alto, Calif.

Kurokawa, T., Tani, Y., Nagata, M. and Nagasaki, R., 2020. Tension and Four-Point Bending Test of Spiral Piles (Twisting a Strip Flat Steel), The 55th Geotechnical Research Presentation, (in Japanese).

Petrasovits, G., Award, A., 1972. Ultimate lateral resistance of a rigid pile in cohesionless soil. Proceedings of 5th European Conference on Soil Mechanics and Foundation Engineering, Madrid, **3**, 407-412.

Prakash, S., 1962. Behavior of pile groups subjected to lateral loads. Ph.D thesis, Univ. of Illinois, Urbana, Ill.

Sato, T., Harada, T., Iwasa, N., Hayashi, S., and Otani, J., 2010. Effect of shaft rotation of spiral piles under its installation on vertical bearing capacity. Japanese Geotechnical Journal, **10**, 2, 253-265. (in Japanese).

Tani, Y., Jugdernamjil, A., Yasufuku, N., Ishikura, R., Kurokawa, T., and Nagata, M., 2020. Horizontal Loading Test of Spiral Piles in Sand. The 55th Geotechnical Research Presentation, (in Japanese).

Verruijt, A., 1995. Computational Geomechanics - Theory and Applications Ch. (8), Kluwer Academic Publishers, Papendrecht, Digital edition.

Yenumula, V. S. N., Prasad. and Chari, T. R., 1999. Lateral capacity of model rigid piles in cohesionless soils. J. Soil and Foundation, **39**, 2, 21-29

Symbols and abbreviations

a	Depth of rotation point
$A_{pipe(front)}$	Frontal projected area of pipe pile
$A_{pipe(side)}$	Side projected area of pipe pile
$A_{Spiral(front)}$	Frontal projected area of spiral pile
$A_{Spiral(side)}$	Side projected area of spiral pile
B	Width of pile
e	Eccentricity of load
E_mI_m	Young's modulus of model pile
E_pI_p	Young's modulus of prototype pile
F	Scale factor
$H_{u(m)}$	Measured ultimate lateral capacity
$H_{u(p)}$	Predicted ultimate lateral capacity
I_m	Model pile second moment of area
K_a	Coefficient of active earth pressure
K_f	Coefficient of friction between the pile and the soil
K_p	Coefficient of passive earth pressure
L	Length of the pile
L_p	Length of the pitch
n_h	Constant horizontal subgrade reaction
p_{max}	Frontal soil resistance
p_u	Ultimate lateral soil pressure
w	Width of spiral wing
α	Rotation angle of pile
γ_d	Unit weight of the soil
δ	Interface friction angle between the pile and the soil
ε	Percentage of error
ζ	Coefficient of rear passive earth pressure
η_{pipe}	Pipe frontal shape factor
η_{spiral}	Spiral frontal shape factor
θ	Angle of a tilted flat bar
ξ_{pipe}	Pipe side shape factor
ξ_{spiral}	Spiral side shape factor
τ_{max}	Side frictional resistance